Ecological Monographs, 79(3), 2009, pp. 445–463
© 2009 by the Ecological Society of America

Modeling the carbon balance of Amazonian rain forests: resolving ecological controls on net ecosystem productivity

R. F. Grant,[1,6] L. R. Hutyra,[2,7] R. C. de Oliveira,[3] J. W. Munger,[2,4] S. R. Saleska,[5] and S. C. Wofsy[2,4]

[1]*Department of Renewable Resources, University of Alberta, Edmonton, Alberta T6G 2E3 Canada*
[2]*Department of Earth and Planetary Sciences, Harvard University, Cambridge, Massachusetts 02138 USA*
[3]*Empresa Brasileira de Pesquisa Agropecuária (EMBRAPA) Amazônia Oriental, Belem PA CEP 66620-270 Brazil*
[4]*School of Engineering and Applied Sciences, Harvard University, Cambridge, Massachusetts 02138 USA*
[5]*Department of Ecology and Evolutionary Biology, University of Arizona, Tuscon, Arizona 85721 USA*

Abstract. There is still much uncertainty about ecological controls on the rate and direction of net CO_2 exchange by tropical rain forests, in spite of their importance to global C cycling. These controls are thought to arise from hydrologic and nutrient constraints to CO_2 fixation caused by seasonality of precipitation and adverse chemical properties of some major tropical soil types. Using the ecosystem model *ecosys*, we show that water uptake to a depth of 8 m avoids constraints to CO_2 and energy exchange from soil drying during five-month dry seasons typical for eastern Amazonian forests. This avoidance in the model was tested with eddy covariance (EC) measurements of CO_2 and energy fluxes during 2003 and 2004 over an old-growth forest on an acidic, nutrient-poor oxisol in the Tapajós National Forest (TNF) in Pará, Brazil. Modeled CO_2 fixation was strongly constrained by slow phosphorus (P) uptake caused by low soil pH. Daytime CO_2 influxes in the model were in close agreement with EC measurements ($R^2 > 0.8$) during both wet and dry seasons. Both modeled and measured fluxes indicated that seasonality of precipitation affected CO_2 and energy exchange more through its effect on radiation and air temperature than on soil water content. When aggregated to a yearly scale, modeled and gap-filled EC CO_2 fluxes indicated that old-growth forest stands in the TNF remained within 100 g $C{\cdot}m^{-2}{\cdot}yr^{-1}$ of C neutrality in the absence of major disturbance. Annual C transformations in *ecosys* were further corroborated by extensive biometric measurements taken in the TNF and elsewhere in the Amazon basin, which also indicated that old-growth forests were either small C sources or small C sinks. Long-term model runs suggested that rain forests could be substantial C sinks for several decades while regenerating after stand-replacing disturbances, but would gradually decline toward C neutrality thereafter. The time course of net ecosystem productivity (NEP) in the model depended upon annual rates of herbivory and tree mortality, which were based on site observations as affected by weather (e.g., El Niño Southern Oscillation [ENSO] events). This dependence suggests that rain forest NEP is strongly controlled by disturbance as well as by weather.

Key words: Brazil; CO_2 exchange; disturbance; ecosys; *ecosystem modeling; net ecosystem productivity; rain forest.*

Introduction

In spite of the importance of CO_2 exchange by Amazonian rain forests to global C cycling, much uncertainty remains about ecological controls on the magnitude and direction of this exchange. Most eddy covariance (EC) studies of CO_2 exchange indicate that these rain forests are C sinks of moderate (100 g $C{\cdot}m^{-2}{\cdot}yr^{-1}$; Grace et al. 1996) to large size (300–700 g $C{\cdot}m^{-2}{\cdot}yr^{-1}$; e.g., Malhi et al. 1998, Andreae et al. 2002, Araújo et al. 2002). However these findings may be affected by inadequate correction for CO_2 emissions suppressed by stable atmospheric conditions that frequently persist during Amazonian nights (Miller et al. 2004). More recent EC studies incorporating this correction indicate that Amazonian rain forests are nearly C neutral (Hutyra et al. 2007). These findings are consistent with biometric studies that indicate that aboveground biomass grows slowly in mature, comparatively undisturbed Amazonian rain forests ($\sim 60 \pm 40$ g $C{\cdot}m^{-2}{\cdot}yr^{-1}$ from a range of mature stands; Phillips et al. 1998, Baker et al. 2004). Some forest stands in the Tapajós National Forest (TNF) in Pará, Brazil have been found to be C sources (80 ± 200 g $C{\cdot}m^{-2}{\cdot}yr^{-1}$, Miller et al. 2004; 190 ± 100 g $C{\cdot}m^{-2}{\cdot}yr^{-1}$, Rice et al. 2004), perhaps because of past disturbances that increased coarse woody debris (CWD) stocks. Variation in net C exchange is also apparent as variation in aboveground living phytomass of old-growth forests (Vieira et al. 2004), complicating efforts

Manuscript received 12 January 2008; revised 3 December 2008; accepted 8 December 2008; final version received 19 January 2009. Corresponding Editor: J. J. Battles.

[6] E-mail: robert.grant@ales.ualberta.ca
[7] Present address: Department of Urban Design and Planning, University of Washington, Seattle, Washington 98195 USA.

to aggregate site estimates of net C exchange to regional scales.

Some of this variation has been attributed to seasonal effects of precipitation, with the dry season either raising (Saleska et al. 2003, Goulden et al. 2004), lowering (Malhi et al. 1998, Araújo et al. 2002, von Randow et al. 2004), or not affecting (Carswell et al. 2002) net CO_2 uptake. The maintenance of rapid CO_2 uptake and transpiration during the dry season has been attributed to deep rooting patterns of Amazonian forests that allow excess precipitation received during the wet season to be transpired during the dry season (Nepstad et al. 1994). Ecosystem models used to calculate net C exchange by rain forests have simulated limitations to CO_2 fixation during the dry season imposed by declining soil water content (θ) that were not apparent in EC measurements (e.g., Tian et al. 1998, Botta et al. 2002), indicating that deep soil hydrology and its effects on net C exchange are not yet being accurately modeled.

Here we test (1) whether the ecosystem model *ecosys* (Grant 2001) can simulate deep rooting under Amazonian conditions using a root submodel in which the vertical distribution of root length is not prescribed, but rather driven by shoot-to-root C transfers governed by access to resources from the atmosphere (O_2), shoot (fixed C), and soil (water, nutrients) (Grant 1998) and (2) whether rooting calculated by this submodel allows *ecosys* to simulate the more rapid CO_2 and energy exchange in EC measurements recorded during the five-month dry season than during the seven-month wet season in the TNF (da Rocha et al. 2004, Goulden et al. 2004, Hutyra et al. 2007). We extend this testing with estimates of seasonal and annual C exchange (wood growth, litterfall, and soil and plant respiration) and of C stocks (living phytomass, CWD) from biometric measurements in the TNF. We then use *ecosys* to examine long-term (100 years) changes in forest net ecosystem productivity (NEP) with forest age and weather following disturbance. This work extends earlier studies of forest age effects on NEP in boreal (Grant et al. 2006*a*, 2007*a*) and temperate (Grant et al. 2007*b*) ecosystems.

Model Development

General

Ecosys is an hourly time-step model with multiple canopy and soil layers that provide a framework for different plant and microbial populations to acquire, transform, and exchange resources (radiation, water, C, N, and P). The model is constructed from algorithms representing basic physical, chemical, and biological processes that determine process rates in plant and microbial populations interacting within complex biomes. These algorithms interact to simulate complex ecosystem behavior across a wide range of spatial and biological scales. The model is designed to represent terrestrial ecosystems under a range of natural and anthropogenic disturbances and environmental changes at patch (spatially homogenous one-dimensional) and landscape (spatially variable two- or three-dimensional) scales. A comprehensive description of *ecosys* with a detailed listing of inputs, outputs, governing equations, parameters, results, and references can be found in Grant (2001). A more detailed description of model algorithms and parameters most relevant to simulating temperature, water, and nutrient effects on rain forest NEP is given below, with reference to equations and variable definitions found in Appendices A, B, and C.

Energy exchange

Ecosystem energy exchange.—Ecosystem temperatures are driven by energy exchanges between the atmosphere and terrestrial surfaces, resolved in *ecosys* into those between the atmosphere and the leaf and stem surfaces of each population (e.g., species or cohort) within the plant community and those between the atmosphere and each of the ground surfaces (soil, surface litter, snow) beneath (Grant et al. 1999). Total energy exchange between the atmosphere and terrestrial surfaces is calculated as the sum of exchanges with all plant and ground surfaces. Surface energy exchange is coupled with soil heat and water transfers, including surface runoff (Manning), infiltration (Green-Ampt), macropore flow (Poiseuille), and micropore flow (Richards) (Grant et al. 2004).

Canopy energy exchange.—Canopy energy exchange in *ecosys* is calculated from an hourly two-stage convergence solution for the transfer of water and heat through a multilayered multi-population soil–root–canopy system. The first stage of this solution requires convergence to a value of canopy temperature (T_c) for each plant population at which the first-order closure of the canopy energy balance (net radiation [Q_n]; sensible heat flux [H]; latent heat flux [LE; Appendix B, Eq. B.1]; and change in heat storage [G]) is achieved. These fluxes are controlled by aerodynamic (r_a) and canopy stomatal (r_c) resistances. Two controlling mechanisms are postulated for r_c that are solved in two successive steps.

First, at the leaf level, leaf resistance, r_l (Appendix C: Eq. C.4), controls gaseous CO_2 diffusion through each leaf surface when calculating CO_2 fixation (Appendix C: Eq. C.1) from concurrent solutions for diffusion, (V_g; Appendix C: Eq. C.2) and carboxylation (V_c; Appendix C: Eq. C.3). The value of r_l is calculated from a minimum leaf resistance (r_{lmin}; Appendix C: Eq. C.5) for each leaf surface that allows a set ratio for intercellular to canopy CO_2 concentration (C_i':C_b) to be maintained at V_c under ambient irradiance, air temperature (T_a), atmospheric CO_2 concentration (C_a), and zero canopy water potential (ψ_c) (V_c'). This ratio will be allowed to vary diurnally as described in *Gross primary productivity* below when ψ_c is solved in the second stage of the convergence solution, described under *Plant water relations* below. Values of r_{lmin} are aggregated by leaf surface area to a canopy value r_{cmin} for use in the energy balance convergence scheme (Appendix B: Eq. B.2).

Second, at the canopy level, r_c rises from r_{cmin} at zero ψ_c from step 1 above through an exponential function of canopy turgor potential (ψ_t; Appendix B: Eq. B.3), calculated from ψ_c and osmotic water potential (ψ_π; Appendix B: Eq. B.4) during convergence for transpiration vs. water uptake.

Plant water relations

After convergence for T_c is achieved, the difference between canopy transpiration (E_c) from the energy balance (Appendix B: Eq. B.1) and total water uptake (U_c; Appendix B: Eq. B.5) from all rooted layers in the soil is tested against the difference between canopy water content from the previous hour and that from the current hour (Appendix B: Eq. B.13). This difference is minimized in each iteration by adjusting ψ_c, which in turn determines each of the three terms in Appendix B: Eq. B.13: (1) E_c (Appendix B: Eq. B.1) through r_c from ψ_t and ψ_π (Appendix B: Eq. B.4), (2) U from the difference between ψ_c and soil water potential (ψ_s) across soil and root hydraulic resistances (Ω_s and Ω_r, respectively) in each rooted soil layer (Appendix B: Eq. B.6), and (3) canopy water content through canopy capacitance (X_c) derived from plant water potential–water content relationships. Root resistances are calculated from root radial and axial resistivities using root lengths and surface areas from a root system submodel driven from shoot–root C transfers (Grant 1998). Because r_c and T_c both drive E_c, the canopy energy balance described under *Energy exchange* above is recalculated for each adjusted value of ψ_c during convergence.

Gross primary productivity

After successful convergence for T_c and ψ_c (described in *Plant water relations* above), V_c is recalculated from that under zero ψ_c (V_c') to that under ambient ψ_c. This recalculation is driven by stomatal effects on V_g (Appendix C: Eq. C.2) from the increase in r_{lmin} at zero ψ_c (Appendix C: Eq. C.5) to r_c at ambient ψ_c (Appendix C: Eq. C.4), and by non-stomatal effects (f_ψ; Appendix C: Eq. C.9) on CO_2-limited carboxylation (V_b; Appendix C: Eq. C.6) and light-limited carboxylation (V_j; Appendix C: Eq. C.7) (Grant and Flanagan 2007). The recalculation of V_c is accomplished through a convergence solution for C_i and its aqueous counterpart (C_c) at which V_g (Appendix C: Eq. C.2) equals V_c (Appendix C: Eq. C.3) (Grant and Flanagan 2007). The CO_2 fixation rate of each leaf surface at convergence is added to arrive at a value for gross primary productivity (GPP) by each plant population in the model (Appendix C: Eq. C.1). The CO_2 fixation product is stored in nonstructural C pools (σ_C) in each branch.

Autotrophic respiration and growth

Carbon oxidation.—The temperature-dependent oxidation of these nonstructural pools (R_c; Appendix C: Eq. C.13) drives autotrophic respiration (R_a; Appendix C: Eq. C.12) by all branches, roots, and mycorrhizae. Oxidation of nonstructural C by roots and mycorrhizae is constrained by O_2 uptake (U_{O2}; Appendix C: Eq. C.13b), calculated by solving for aqueous O_2 concentrations at root and mycorrhizal surfaces ($[O_{2r}]$) at which convection and radial diffusion through the soil aqueous phase plus radial diffusion through the root aqueous phase (Appendix C: Eq. C.13d) equals active uptake driven by O_2 demand from R_c (Appendix C: Eq. C.13c) (Grant 2004). The diffusion processes are driven by aqueous O_2 concentrations sustained by transport and dissolution of gaseous O_2 through soil and roots (Grant 2004) and are governed by lengths and surface areas of roots and mycorrhizae (Grant 1998). Thus R_c is coupled to O_2 reduction by all root and mycorrhizal populations according to O_2 availability.

Plant maintenance and growth.—Oxidation of nonstructural C is first used to meet maintenance respiration requirements (R_m; Appendix C: Eq. C.15), then any excess is expended as growth respiration (R_g) constrained by branch, root, or mycorrhizal ψ_t (Appendix C: Eq. C.16). Growth respiration drives the conversion of branch σ_C into foliage, twigs, branches, boles, and reproductive material according to organ growth yields (Y_g) and phenology-dependent partitioning coefficients (Appendix C: Eq. C.19) and the conversion of root and mycorrhizal σ_C into primary and secondary axes according to root and mycorrhizal growth yields. Because branch ψ_t is usually lower than root ψ_t, branch R_g declines relatively more with soil drying than does root R_g, slowing oxidation of σ_C in branches and allowing more translocation of σ_C from branches to roots. This change in allocation of σ_C enables more root growth to reduce Ω_s, Ω_r, and Ω_a and hence increase U (Appendix B: Eq. B.6), thereby offsetting the effects of soil drying on ψ_t. Translocation of σ_C thus maintains a functional equilibrium among branches, roots, and mycorrhizae that adapts to changing hydrology.

Maintenance respiration is calculated independently of R_c from the N content in each organ and a function of T_c or soil temperature (T_s: Appendix C: Eq. C.15). When R_m exceeds R_c, the shortfall is met by the respiration of remobilizable C (R_s) in leaves and twigs or roots and mycorrhizae (Appendix C: Eq. C.14). Respiration of remobilizable C drives the withdrawal of remobilizable C, N, and P (mostly nonstructural protein) from leaves and twigs or roots and mycorrhizae into σ_N and σ_P and the loss of associated non-remobilizable C, N, and P (mostly structural) as litterfall (Appendix C: Eq. C.17). Provision is also made to withdraw remobilizable N or P from leaves and twigs or roots and mycorrhizae when ratios of σ_N:σ_C or σ_P:σ_C become smaller than those required for growth of new phytomass. This withdrawal drives the withdrawal of associated remobilizable C and the loss of associated non-remobilizable C, N, and P as litterfall. Environmental constraints such as water, heat, nutrient, or O_2 stress that reduce σ_C and hence R_c with respect to R_m therefore hasten litterfall.

Autotrophic respiration of each branch or root and mycorrhizal layer is the total of R_c and R_s, and net primary productivity (NPP) is the difference between canopy GPP (Appendix C: Eq. C.1) and total R_a of all branches and root and mycorrhizal layers (Appendix C: Eq. C.12). Phytomass net growth is the difference between gains driven by R_g and Y_g and losses driven by R_s and litterfall (Appendix C: Eq. C.19). These gains are allocated to leaves, twigs, wood, and reproductive material at successive branch nodes and to roots and mycorrhizae at successive primary and secondary axes, driving growth in plant stature. Losses from remobilization and litterfall in shoots start at the lowest node of each branch at which leaves or twigs are present and proceed upwards when leaves or twigs are lost. Losses in roots and mycorrhizae start with secondary axes and proceed to primary axes when secondary axes are lost.

Nutrient uptake and translocation

Root and mycorrhizal uptake.—Root and mycorrhizal uptake of N and P U_{NH_4}, U_{NO_3}, and U_{PO_4} is calculated by solving for solution $[NH_4^+]$, $[NO_3^-]$, and $[H_2PO_4^-]$ at root and mycorrhizal surfaces at which radial transport by mass flow and diffusion from the soil solution to these surfaces (Appendix A: Eq. A.36a, c, e] equals active uptake by the surfaces (Appendix A: Eq. A.36b, d, f). Path lengths and surface areas for U_{NH_4}, U_{NO_3}, and U_{PO_4} are calculated from a root and mycorrhizal growth submodel (Grant 1998). Solution $[NH_4^+]$, $[NO_3^-]$, and $[H_2PO_4^-]$ are controlled by precipitation, adsorption, and ion pairing reactions (Grant and Heaney 1997, Grant et al. 2004). If pH is assumed constant in the model, then only a subset of these reactions that directly control NH_4^+, NO_3^-, and $H_2PO_4^-$ solubility are solved, including precipitation-dissolution of $Al(OH)_3$, $Fe(OH)_3$, $CaCO_3$, $AlPO_4$, $FePO_4$, $Ca(H_2PO_4)_2$, $CaHPO_4$, and $Ca_5(PO_4)_3OH$, cation exchange between Ca^{2+} and NH_4^+, anion exchange between adsorbed $H_2PO_4^-$ and HPO_4^{2-} and soluble $H_2PO_4^-$, and ion pairing between NH_4^+ and NH_3. Solution $[NH_4^+]$, $[NO_3^-]$, and $[H_2PO_4^-]$ are also controlled by vertical and horizontal solute transport (Grant et al. 2004) and by microbial activity including mineralization, nitrification, denitrification, volatilization, and N_2 fixation described under *Heterotrophic respiration* below.

Translocation.—Products of U_{NH_4}, U_{NO_3}, and U_{PO_4} are added to σ_N and σ_P in root and mycorrhizal layers where they are coupled with σ_C to drive growth of branches, roots, and mycorrhizae as described in *Autotrophic respiration and growth* above. The translocation of σ_C, σ_N, and σ_P among branches and root and mycorrhizal layers is driven by concentration gradients generated by production of σ_C from branch GPP and of σ_N and σ_P from root and mycorrhizal uptake vs. consumption of σ_C, σ_N, and σ_P from R_c, R_g, and phytomass growth (Grant 1998). Low σ_N:σ_C or σ_P:σ_C in branches indicate excess CO_2 fixation with respect to N or P uptake for phytomass growth. Such ratios in the model have two effects on GPP: (1) They reduce activities of rubisco (Appendix C: Eq. C.6a) and chlorophyll (Appendix C: Eq. C.7a) through product inhibition (Appendix C: Eq. C.11), thereby simulating the suppression of CO_2 fixation by leaf σ_C accumulation widely reported in the literature. (2) They reduce the structural N:C and P:C ratios at which leaves are formed because σ_C, σ_N, and σ_P are the substrates for leaf growth. Lower structural ratios cause a proportional reduction in areal concentrations of rubisco (Appendix C: Eq. C.6b) and chlorophyll (Appendix C: Eq. C.7b), reducing leaf CO_2 fixation.

Low σ_N:σ_C or σ_P:σ_C in mycorrhizae and roots indicates inadequate N or P uptake with respect to CO_2 fixation. These ratios affect translocation of σ_C, σ_N, and σ_P by lowering mycorrhizal–root–branch concentration gradients of σ_N and σ_P while raising branch–root–mycorrhizal concentration gradients of σ_C. These changes slow transfer of σ_N and σ_P from root to branch and hasten transfer of σ_C from branch to root, increasing root and mycorrhizal growth at the expense of branch growth and thereby raising N and P uptake with respect to CO_2 fixation. High σ_N:σ_C or σ_P:σ_C in roots and mycorrhizae indicate excess N or P uptake with respect to CO_2 fixation. Such ratios reduce specific activities of root and mycorrhizal surfaces for N or P uptake through a product inhibition function, as has been observed experimentally. Thus the modeled plant translocates σ_C, σ_N, and σ_P among branches, roots, and mycorrhizae to maintain a functional equilibrium between acquisition and use of C, N, and P by different parts of the plant.

Heterotrophic respiration

Decomposition.—Organic transformations in *ecosys* occur in five organic matter–microbe complexes (coarse woody litter, fine nonwoody litter, animal manure [if present], particulate organic matter [POM], and humus) in each soil layer. Each complex consists of five organic states: solid organic matter, dissolved organic matter, sorbed organic matter, microbial biomass, and microbial residues, among which C, N, and P are transformed. Organic matter in litter and manure complexes are partitioned from proximate analysis results into carbohydrate, protein, cellulose, and lignin components of differing vulnerability to hydrolysis. Organic matter in POM, humus, microbial biomass, and microbial residues in all complexes are also partitioned into components of differing vulnerability to hydrolysis.

The rate at which each component of each organic state in each complex is hydrolyzed during decomposition is a first-order function of the active biomass, M, of all heterotrophic microbial populations (Appendix A: Eqs. A.1, A.2). The rate at which each component is hydrolyzed is also a Monod function of substrate concentration (Appendix A: Eqs. A.3, A.4]), calculated from the fraction of substrate mass colonized by M. Hydrolysis rates are controlled by T_s through an Arrhenius function [A5] and by soil water content (θ)

PLATE 1. Flux tower view at the study site in Amazonian Tapajós National Forest. Photo credit: L. R. Hutyra.

through its effect on aqueous concentrations of active microbial biomass [M] (Appendix A: Eqs. A.3, A.4) in surface litter and in a spatially resolved soil profile. Soil temperature and θ are calculated from surface energy balances and from heat and water transfer schemes through canopy–snow–residue–soil profiles as described in *Energy exchange* above. Release of N and P from hydrolysis of each component in each complex is determined by its N and P concentrations (Appendix A: Eqs. A.6, A.7), which are determined from those of the originating litterfall as described in *Autotrophic respiration and growth* above. Most non-lignin hydrolysis products are released as dissolved organic C, N, and P (DOC, DON, and DOP), which are adsorbed or desorbed according to a power function of their soluble concentrations (Appendix A: Eqs. A.8–A.10).

Microbial growth.—The DOC decomposition product is the substrate for heterotrophic respiration, R_h, by all M in each substrate–microbe complex (Appendix A: Eq. A.13). Total R_h for all soil layers (Appendix A: Eq. A.11) drives CO_2 emission from the soil surface through volatilization and diffusion. Heterotrophic respiration may be constrained by microbial N or P concentrations, T_s, DOC, and O_2 (Appendix A: Eqs. A.12–A.14). O_2 uptake by M is driven by R_h (Appendix A: Eq. A.15) and constrained by O_2 diffusivity to microbial surfaces (Appendix A: Eq. A.16), as described for roots in *Autotrophic respiration and growth* above. Thus R_h is coupled to O_2 reduction by all aerobic M according to O_2 availability. Heterotrophic respiration not coupled with O_2 reduction is coupled with the sequential reduction of NO_3^-, NO_2^-, and N_2O by heterotrophic denitrifiers and with the reduction of organic C by fermenters and acetotrophic methanogens. In addition, autotrophic nitrifiers conduct NH_4^+ and NO_2^- oxidation and NO_2^- reduction, and autotrophic methanogens and methanotrophs conduct CH_4 production and oxidation.

All microbial populations undergo maintenance respiration R_m (Appendix A: Eqs. A.17, A.18), depending on microbial N and T_s as described earlier for plants. Heterotrophic respiration in excess of R_m is used in growth respiration (R_g; Appendix A: Eq. A.19), the energy yield (ΔG) of which drives growth in biomass (M) from DOC uptake according to the energy requirements of biosynthesis (Appendix A: Eqs. A.20, A.21). Maintenance respiration in excess of R_h causes microbial dieback. Biomass also undergoes first-order decomposition (D_m; Appendix A: Eq. A.22). Internal retention and recycling of microbial N and P during decomposition (Appendix A: Eq. A.23) is modeled whenever these nutrients constrain R_h (Appendix A: Eq. A.12). Changes in M arise from differences between gains from DOC uptake and losses from $R_m + R_g + D_m$ (Appendix A: Eq. A.24).

Microbial nutrient exchange.—During these changes, all microbial populations seek to maintain set minimum ratios of C:N or C:P in M by mineralizing or immobilizing NH_4^+, NO_3^-, and $H_2PO_4^-$ (Appendix A: Eq. A.25), thereby controlling solution [NH_4^+], [NO_3^-],

TABLE 1. Representative physical and chemical properties of nutrient-poor clay oxisols measured in the Tapajós National Forest in Pará, Brazil, and used in the ecosystem model *ecosys*.

Property	Layer (m)							
	1	2	3	4	5	6	7	8
Depth to bottom (m)	0.075	0.225	0.375	0.625	1.375	2.625	4.375	10.375
Bulk density (Mg/m^3)	1.16	1.24	1.26	1.21	1.22	1.26	1.26	1.26
Sand (g/kg)	588	515	467	426	418	430	430	430
Silt (g/kg)	20	30	30	0	0	0	0	0
Clay (g/kg)	392	455	503	574	582	570	570	570
Coarse fragments (m^3/m^3)	0	0	0	0	0	0	0	0
pH	3.72	4.08	4.08	4.35	4.35	4.35	4.35	4.35
CEC ($cmol^{(+)}/kg$)	5	5	5	5	5	5	5	5
AEC ($cmol^{(-)}/kg$)	3	3	3	3	3	3	3	3
Organic C (g/kg)	21.8	7.85	7.85	3.88	2.0	1.0	0.5	0.0
Total N (g/Mg)	1500	920	920	454	200	100	50	0
Total P (g/Mg)	215	140	140	110	90	80	80	80
Exchangeable P (g/Mg)	3.4	1	1	0	0	0	0	0

Notes: For all properties except depth to bottom, coarse fragments, and AEC, values to 1 m are from Silver et al. (2000); values below 1 m are assumed to be the same as those above 1 m. Values for AEC are from Falcão and da Silva (2004). Abbreviations are: CEC, cation exchange capacity; AEC, anion exchange capacity.

and [$H_2PO_4^-$] that determine root and mycorrhizal uptake in *Nutrient uptake and translocation* above. If immobilization is inadequate to maintain these minimum ratios, then biomass C:N or C:P may rise, but R_h is constrained by N or P present in the lowest concentration with respect to that at the minimum ratio (Appendix A: Eq. A.12). Non-symbiotic heterotrophic diazotrophs can also fix aqueous N_2 (Appendix A: Eq. A.26) to the extent that immobilization is inadequate to maintain their set minimum C:N, but at an additional respiration cost (Appendix A: Eq. A.27). Changes in microbial N and P arise from DON and DOP uptake plus NH_4^+, NO_3^-, and $H_2PO_4^-$ immobilization and N_2 fixation, less NH_4^+, NO_3^-, and $H_2PO_4^-$ mineralization and microbial N and P decomposition (Appendix A: Eq. A.28).

Humification.—Carbon, N, and P decomposition products in each organic matter–microbe complex are gradually stabilized into more recalcitrant organic forms with lower C:N and C:P ratios. Products from lignin hydrolysis (Appendix A: Eqs. A.1, A.6) combine with some of the products from protein and carbohydrate hydrolysis in the litterfall and manure complexes and are transferred to the POM complex (Appendix A: Eqs. A.30–A.33). Microbial decomposition products (Appendix A: Eqs. A.22, A.23) from all complexes are partitioned between the humus complex and microbial residues in the originating complex according to soil clay content (Appendix A: Eqs. A.34, A.35).

FIELD EXPERIMENT

Site description

Experimental work to study net C exchange by Amazonian rain forests was conducted at a site within the Tapajós National Forest (TNF), ~7 km from the 67-km road marker on the Santarém-Cuiaba Highway (hereafter "Santarém km 67"), ~70 km south of Santarém (54°58′ W, 2°51′ S; see Plate 1). The TNF is a 450 000-ha area of closed-canopy upland forest with a mean temperature of 25°C and relative humidity of 85%. The forest receives mean annual rainfall of 1909 mm, with a five-month dry season between July and November. The forest is on flat terrain and has a closed canopy with a mean height of ~40–45 m and emergent trees reaching up to 55 m. There are few indications of recent anthropogenic disturbance other than small hunting trails. This forest can be classified as "primary" with abundant large logs, numerous epiphytes, an uneven age distribution, and emergent trees. The soils are nutrient-poor clay oxisols, with low organic matter, exchangeable P, and cation exchange capacity (Table 1; Silver et al. 2000).

Biometric measurements

Four transects totaling 19.75 ha were established during July 1999 to measure C stocks in primary forest areas near Santarém km 67. Three additional transects totaling 30 ha were established during 2003 near km 72 and km 117 along the Santarém-Cuiaba highway. The transects were designed to capture spatial variations inherent in tropical forests, including those of the common emergent species *Manilkara huberi* (Ducke) Chev., *Hymanaea courbaril* L., and *Tachigalia* spp., considered typical for the region. Locations and sampling protocols and allometric methods for living phytomass and CWD measurements in plots established along these transects were described in Rice et al. (2004) and Pyle et al. (2008).

Eddy covariance measurements

A 64-m EC tower was operated from April 2001 to January 2006 ~6 km west of the 67 km road marker on the BR-163 highway and ~6 km east of the Tapajós River, in an area of largely contiguous forest extending for tens of kilometers to the north and south. All key instruments and data loggers were mounted at 57.8 m on the tower to keep inlet tubes short (~2 m) in this tall canopy. Flux measurements recorded at 8 Hz were

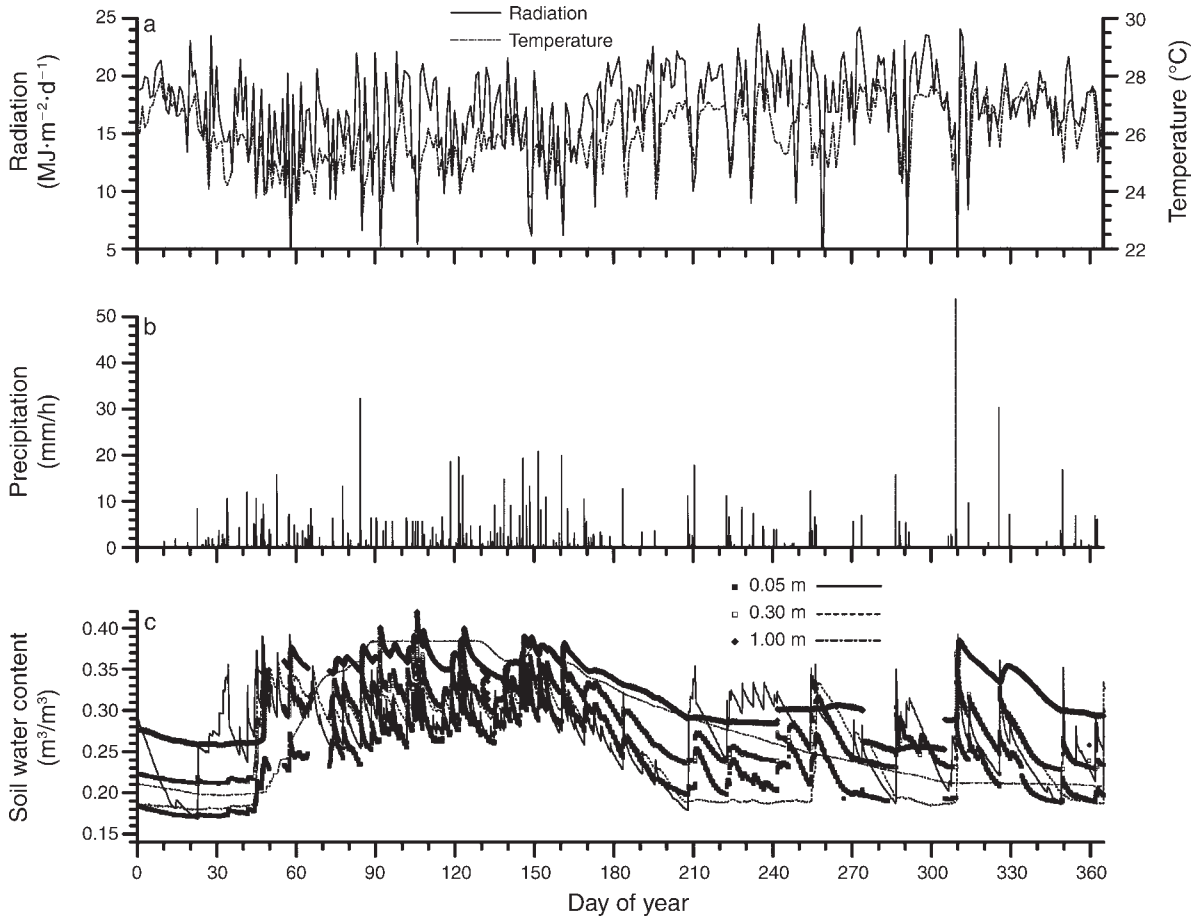

FIG. 1. (a) Daily total radiation and mean air temperature, (b) hourly precipitation, and (c) hourly soil water content (θ) modeled (lines) and measured (symbols) at Santarém km 67 within the Tapajós National Forest (TNF) in Pará, Brazil, during 2003.

averaged to half-hour values, excluding those recorded at a friction velocity (u^*) of <0.22 m/s. The EC measurement protocol is described further in Hutyra et al. (2007) and Saleska et al. (2003). In addition, vertical profiles of CO_2 and H_2O concentrations were measured at eight levels on the tower (62.2, 50, 39.4, 28.7, 19.6, 10.4, and 0.91 m) to estimate half-hourly changes in canopy CO_2 and energy storage that were added to EC fluxes for comparison with model output.

Soil water contents (θ) were measured every half-hour using time domain reflectometry (TDR) probes (CS-615; Campbell Scientific, Logan, Utah, USA) at depths of 0.05, 0.15, 0.30, 0.50, 1.0, and 2.0 m in each of three locations near the flux tower.

Model Experiment

Ecosys was run with the physical and chemical properties of the nutrient-poor clay oxisols typical of the experimental site (Table 1; Silver et al. 2000) and the biological properties of overstory and understory plant populations in an evergreen tropical rain forest (see Appendices B and C). These biological properties were identical to those in earlier studies of boreal and temperate broadleaf forests (Hanson et al. 2004, Grant et al. 2006*a*, *b*, 2007*a*, *b*), except that (1) the deciduous growth habit, in which photoperiod- and temperature-dependent algorithms remobilize overwinter reserves during "leaf-out" and rebuild overwinter reserves during leaf fall, was suppressed so as to simulate an evergreen growth habit; (2) the zone of thermal adaptation was changed from boreal or temperate to tropical by shifting the temperature functions for microbial activity (Appendix A: Eq. A.5), V_c (Appendix C: Eq. C.10), R_c (Appendix C: Eq. C.13), and R_m (Appendix C: Eq. C.15) to the right by 3°C for each 10°C rise in annual mean temperature. This shift raised temperature optima for these processes based on relationships of growth temperatures with temperature responses of carboxylation found in a meta-analysis by Medlyn et al. (2002) and with those of respiration in several studies reported in Larcher (2001).

Ecosys was initialized with CWD stocks of 10 kg C/m^2 (standing) and 5 kg C/m^2 (surface), representing stocks remaining after a stand-replacing disturbance. *Ecosys* was seeded with an evergreen overstory and understory and run during model years 1900 to 2005 with repeating cycles

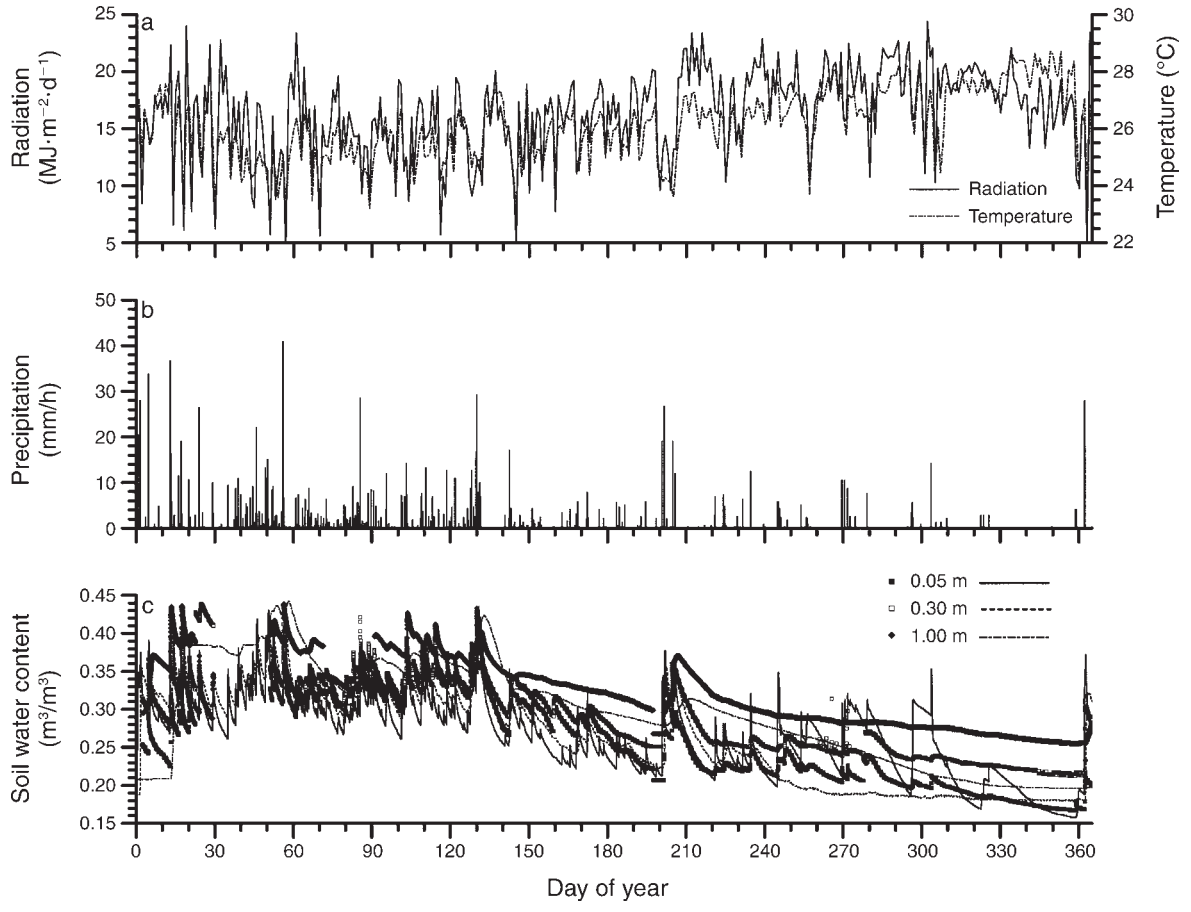

FIG. 2. (a) Daily total radiation and mean air temperature, (b) hourly precipitation, and (c) hourly soil water content (θ) modeled (lines) and measured (symbols) at Santarém km 67 during 2004.

of hourly weather data (radiation, T_a, dewpoint, wind speed, and precipitation) recorded at the EC tower during 2002–2005. This period allowed the simulated forest to regenerate, mature, and attain dynamic C equilibrium well before the end of the model run so as to permit comparison with the old-growth forest in the TNF. During the model run, atmospheric CO_2 concentration (C_a) was initialized at 275 μmol/mol and raised hourly at an annual rate of 0.3%, reaching current C_a by the end of the run. Concentrations of NH_4^+-N, NO_3^--N, and $H_2PO_4^-$-P in precipitation remained at 0.1, 0.05, and 0.01 g/m^3, respectively, during the model run so as to approximate precipitation concentrations measured by Lesack and Melack (1991) in the central Amazon. A background mortality rate of 2% per year, based on C stock measurements at Santarem by Pyle et al. (2008), was applied monthly during each year of the model run. This rate was raised to 6% per year during El Niño Southern Oscillation (ENSO) years (1903, 1912, 1917, 1926, 1931, 1935, 1940, 1956, 1965, 1974, 1983, 1988, 1993, and 1998), based on a review of ENSO-caused mortality in tropical forests by Clark (2004) and on estimates from CWD measurements at Santarem by Pyle et al. (2008). Mortality events were simulated by removing all plant material from specified fractions of remaining plant populations and adding nonwoody material (leaves, twigs, reproductive material, fine roots, mycorrhizae) to surface and subsurface fine-litter stocks and adding woody material (boles, coarse roots) to standing dead and subsurface CWD stocks. In addition, herbivory was simulated as daily removals of standing leaf mass to give annual removals of 10%, consistent with those summarized for tropical rain forests by Coley and Barone (1996). Herbivory products were added as litterfall to surface stocks of fine litter and manure. Exchanges of CO_2 and energy and transformations of phytomass and litter stocks simulated during 2003–2005 of the model run were compared with EC and biometric measurements recorded near Santarém km 67 during 2003–2005. Model performance was evaluated through regression analyses in which agreement between measured and modeled fluxes of LE and CO_2 was indicated by slopes and intercepts not greatly different from 1 and 0, respectively. Based on random errors in EC flux measurements derived over forested sites by Richardson et al. (2006), slopes and intercepts within 0.1 of 1 and within 15 W/m^2 (LE) or 1 μmol·m^{-2}·s^{-1} (CO_2) of 0 could be considered acceptable. Agreement was also indicated by root mean squares for

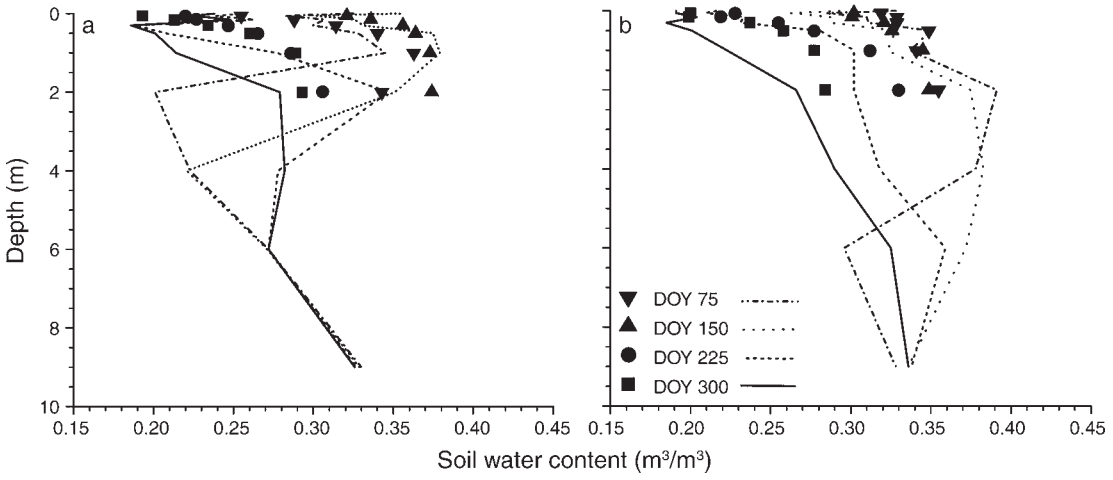

FIG. 3. Vertical profiles of soil water content (θ) measured (symbols) and modeled (lines) during the wet season (day of year [DOY] 75 and 150) and dry season (DOY 225 and 300) at Santarém km 67 in (a) 2003 (modeled vs. measured $R^2 = 0.69$, root mean squares for differences [RMSD] = 0.034 m^3/m^3) and (b) 2004 (modeled vs. measured $R^2 = 0.84$, RMSD = 0.024 m^3/m^3).

differences (RMSD) between measured and modeled fluxes not significantly greater than root mean squares for error (RMSE) in the measured fluxes derived over forest stands by Richardson et al. (2006).

RESULTS

Forest hydrology

Soil water uptake.—Dry-season (15 July–15 December) and wet-season (15 December–15 July) precipitation were comparatively low during 2002–2003 (279 and 1316 mm, respectively) and high during 2003–2004 (424 and 1904 mm, respectively), allowing model behavior to be studied under contrasting hydrological conditions during 2003 and 2004. Radiation (Q) and T_a declined during the wet seasons and rose during the dry (Figs. 1a and 2a). Frequent rains during early 2003 (Fig. 1b) caused measured and modeled θ to rise during February (Fig. 1c). The following dry season (Fig. 1b) caused θ to decline at progressively greater depths from July to November, although near-surface θ was temporarily raised by infrequent rainfall (Fig. 1c). More precipitation during the following wet season (Fig. 2b) caused θ to rise earlier during 2004 (Fig. 2c). However, a protracted dry season later in 2004 caused soil drying to persist until the end of the year.

Low precipitation during 2002–2003 caused a zone of drier soil to be modeled at 4 m in early 2003 (Fig. 3a). Water in this zone was replenished by higher precipitation during 2003–2004 (Fig. 3b). Soil water uptake in the model extended to a depth of 8 m during 2004, although most occurred within the upper 4 m. The depth of soil drying in the model was similar to that measured by Bruno et al. (2006) at a nearby site in the TNF where drying extended to a depth of 10 m in 2002 following two years of comparatively low precipitation. Soil water uptake in the model was driven by root length densities (as described in *Plant water relations* above) that declined exponentially with depth to 9 m. Values of RMSD from regressions of measured on modelled θ during 2003 and 2004 (Fig. 3) were not significantly greater than RMSE from regressions of measured θ on TDR probe readings during calibration that varied from 0.02 to 0.05 m^3/m^3 among different probes and depths, indicating no significant disagreement between modeled and measured θ.

Energy exchange.—Rises in Q and T_a during the dry season (Figs. 1a and 2a) caused modeled LE to rise from midday rates of 200–400 W/m^2 under variable Q_n during the late wet season of 2004 (Fig. 4a) to midday rates of 400 W/m^2 under sustained Q_n during the late dry season (Fig. 4b), consistent with the EC measurements. These rises in LE were driven by rises in vapor pressure deficit (D) during the dry season (Fig. 4c, d). However, modeled rises in LE were constrained by midafternoon declines in canopy stomatal conductance, g_c, when D rose above 1.5 kPa (e.g., days of year [DOY] 294–295 and 299 in Fig. 4d) as observed experimentally in the TNF by da Rocha et al. (2004). Midday g_c in the model was similar to means of 13 and 12 mm/s for wet and dry seasons calculated in the TNF by da Rocha et al. (2004) from EC flux measurements and an inverted Penman-Monteith equation. These g_c were sustained by comparatively high ψ_c in the model, predawn values of which declined little from −0.4 MPa in the wet season to −0.5 MPa in the dry season, consistent with earlier measurements in the TNF by Nepstad et al. (2002).

In both years, modeled LE explained ~80% of variation in EC values, with little bias ($a \rightarrow 0$, $b \rightarrow 1$; Table 2). The RMSD between modeled and measured LE fluxes were similar to random errors in EC LE fluxes of 50–60 W/m^2 estimated from measurements over tall temperate forests by Richardson et al. (2006) for the range of LE fluxes measured in the TNF.

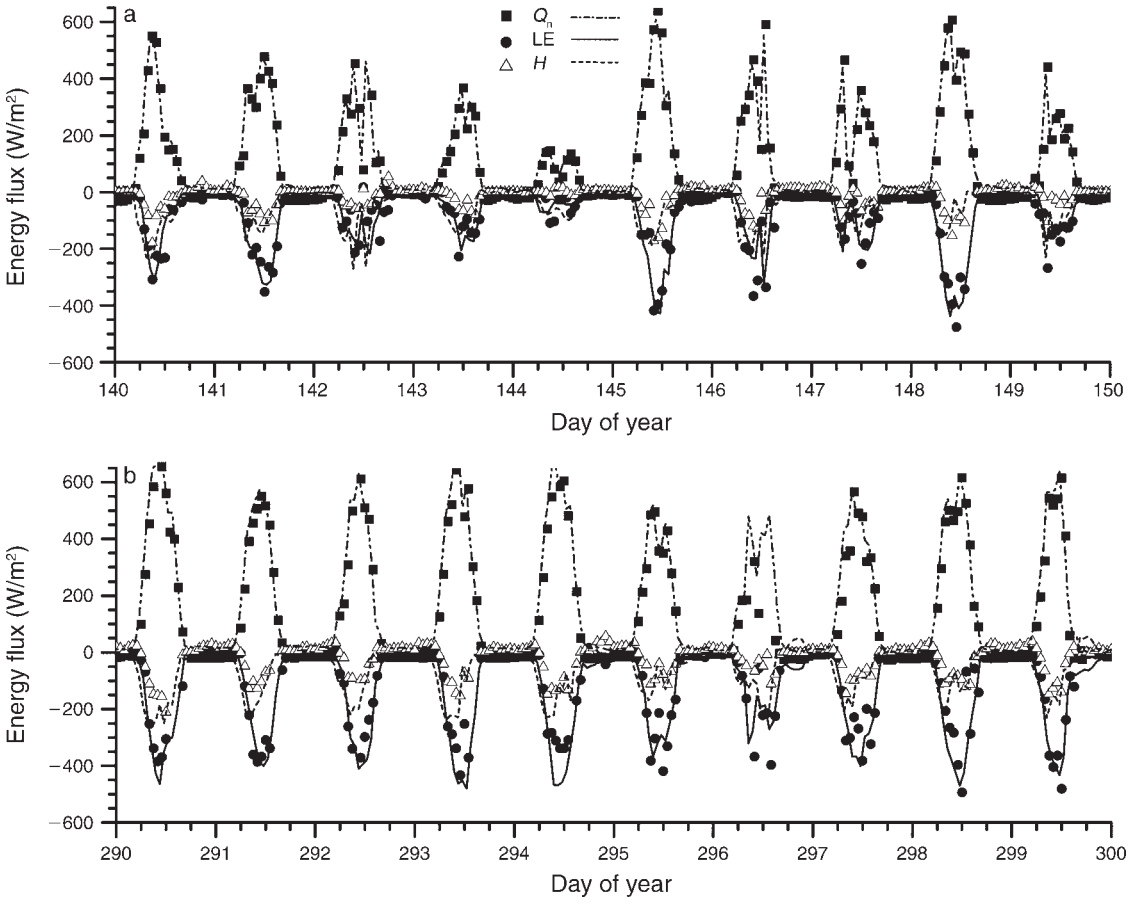

FIG. 4. (a, b) Net radiation (Q_n), latent heat (LE), and sensible heat (H) measured (symbols) and modeled (lines) during (a) the late wet season (day of year [DOY] 141–150) and (b) the late dry season (DOY 290–300) at Santarém km 67 in 2004. Positive values represent downward fluxes, negative value upward ones. (c, d) [next page] Vapor pressure deficit (D) measured and canopy stomatal conductance (g_c) modeled during (c) the late wet season and (d) the late dry season at Santarém km 67 in 2004.

CO_2 exchange.—More rapid LE vs. H from both EC measurements and the model (Fig. 4) indicated that plant water status did not much constrain CO_2 fixation during either the wet or the dry season, as apparent in maximum CO_2 influxes of ~20 μmol·m^{-2}·s^{-1} measured and modeled during both seasons in 2004 (Fig. 5a, b). Small midafternoon declines were modeled on days with higher D and hence lower g_c (DOY 294–295 and 299; Fig. 4d), simulating the slight negative correlation between D and CO_2 influxes found by Malhi et al. (1998). Although modeled CO_2 influxes were usually within 2 μmol·m^{-2}·s^{-1} of EC values, modeled CO_2 effluxes were sometimes larger than EC values by as much as 5 μmol·m^{-2}·s^{-1}, even when $u^* > 0.22$ m/s (e.g., DOY 297–298; Fig. 5b). When $u^* < 0.22$ m/s, modeled CO_2 effluxes were often larger than gap-filled estimates that replaced EC measurements during dry seasons when CO_2 influxes were larger. In both years, modeled CO_2 fluxes explained >80% of variation in EC measurements (excluding gap-filled values), with little bias ($a \rightarrow 0$, $b \rightarrow 1$; Table 2). The RMSD between modeled and measured CO_2 fluxes were similar to random errors in EC CO_2 flux measurements of 2.5–4.5 μmol·m^{-2}·s^{-1} estimated over temperate forests by Richardson et al. (2006) for the range of CO_2 fluxes measured in the TNF.

In the model, CO_2 uptake was constrained by low nonstructural σ_P:σ_C in leaves (Appendix C: Eq. C.11) caused by slow uptake of P by roots caused in turn by low [$H_2PO_4^-$] in the soil (Appendix A: Eq. A.36; see also *Nutrient uptake and translocation* above). Low soil [$H_2PO_4^-$] in the model was caused by low pH (Table 1), which forced precipitation of $H_2PO_4^-$ as $AlPO_4$ and $FePO_4$, and increased protonated anion exchange sites and hence $H_2PO_4^-$ adsorption, as found experimentally (Gehring et al. 1999, McGrath et al. 2001). Leaf σ_P:σ_C ratios in the model declined with advancing forest age, causing foliar and litterfall P:C ratios to fall below 0.003 and 0.0006, respectively, by 100 years after a stand-replacing disturbance when model CO_2 fluxes in Fig. 5 were generated. These P:C ratios were typical of those found by Vitousek and Sanford (1986) and Silver et al. (2000) for P-limited tropical forests growing on nutrient-poor oxisols in the TNF and elsewhere. Leaf P:N ratios in the model declined to 0.045, smaller than values of

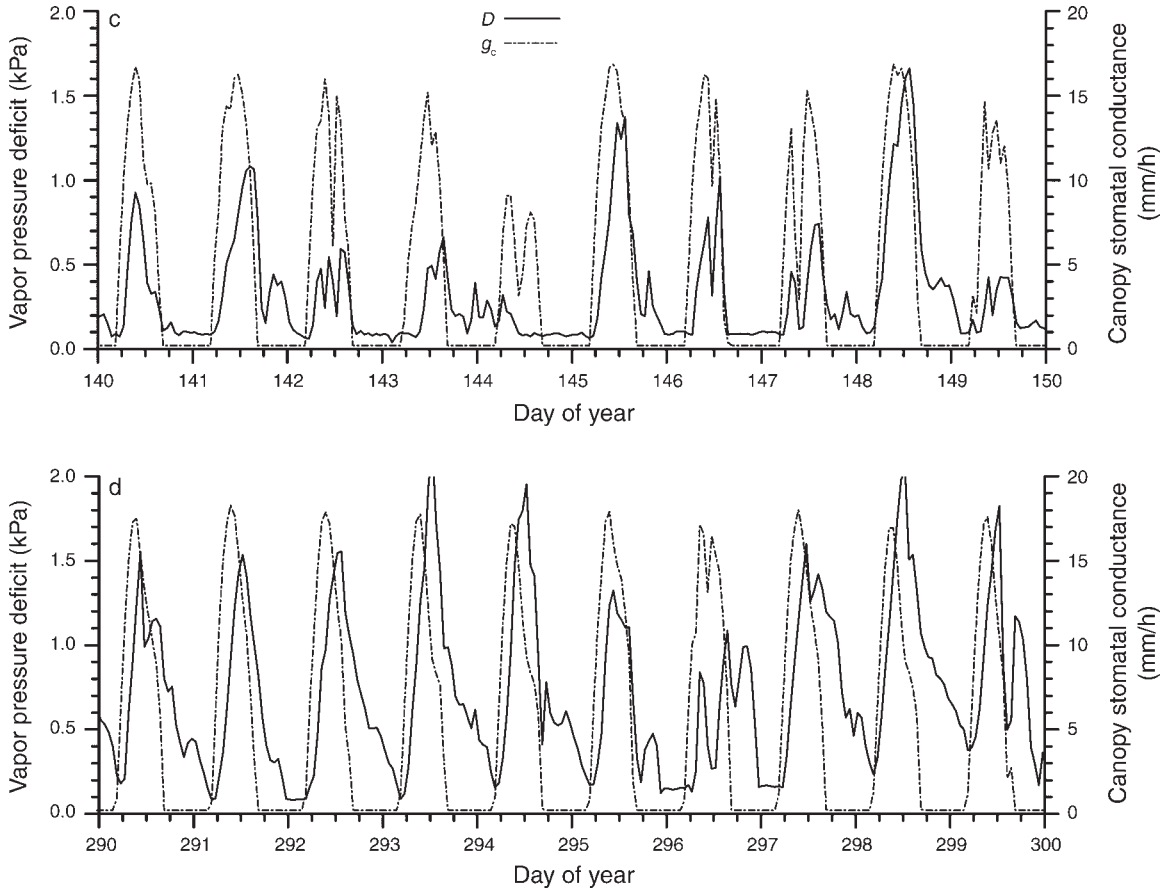

FIG. 4. Continued.

0.06 found in P-limited tropical forests by Harrington et al. (2001). Low litterfall P:C and P:N in turn forced immobilization of $H_2PO_4^-$ by heterotrophic microbial populations during litter decomposition (Appendix A: Eq. A.25), as found experimentally in the TNF by McGroddy et al. (2004). Immobilization further limited root P uptake while retaining P in the organic phase for eventual remineralization.

Seasonal evapotranspiration and net ecosystem productivity.—The rise in hourly LE modeled and measured during the dry season (15 July–15 December; Fig. 4) was apparent as a rise in daily evapotranspiration (ET) from variable rates of ~3 mm/d during the wet season to ones of ~4 mm/d during the dry season in 2003 (Fig. 6a) and 2004 (Fig. 7a). A similar rise in ET has been measured elsewhere in the TNF by da Rocha et al. (2004). These rises were accompanied by ones in NEP from <0 g $C \cdot m^{-2} \cdot d^{-1}$ (net C source) during the later wet season to >0 g $C \cdot m^{-2} \cdot d^{-1}$ (net C sink) during the dry season (Figs. 6b and 7b). These rises in ET and NEP from the wet to

TABLE 2. Statistics from regressions of simulated on measured (*a, b*) and measured on simulated (R^2, RMSD) hourly latent heat flux (LE) and CO_2 fluxes over an old-growth rain forest at Santarém km 67.

Year	*n*	*a*†	*b*†	R^2‡	RMSD‡
LE (W/m^2)					
2003	5043	−22	0.94	0.83	57
2004	4642	−28	0.91	0.77	66
CO_2 ($\mu mol \cdot m^{-2} \cdot s^{-1}$)					
2003	4744	0.72	0.90	0.85	4.4
2004	3998	0.88	0.94	0.82	4.7

Note: All measured values were recorded at a friction velocity of $u^* > 0.2$ m/s.
† $Y = a + bX$ from regression of simulated Y on measured X.
‡ R^2, coefficient of determination; RMSD, root mean square for error from regression of measured Y on simulated X.

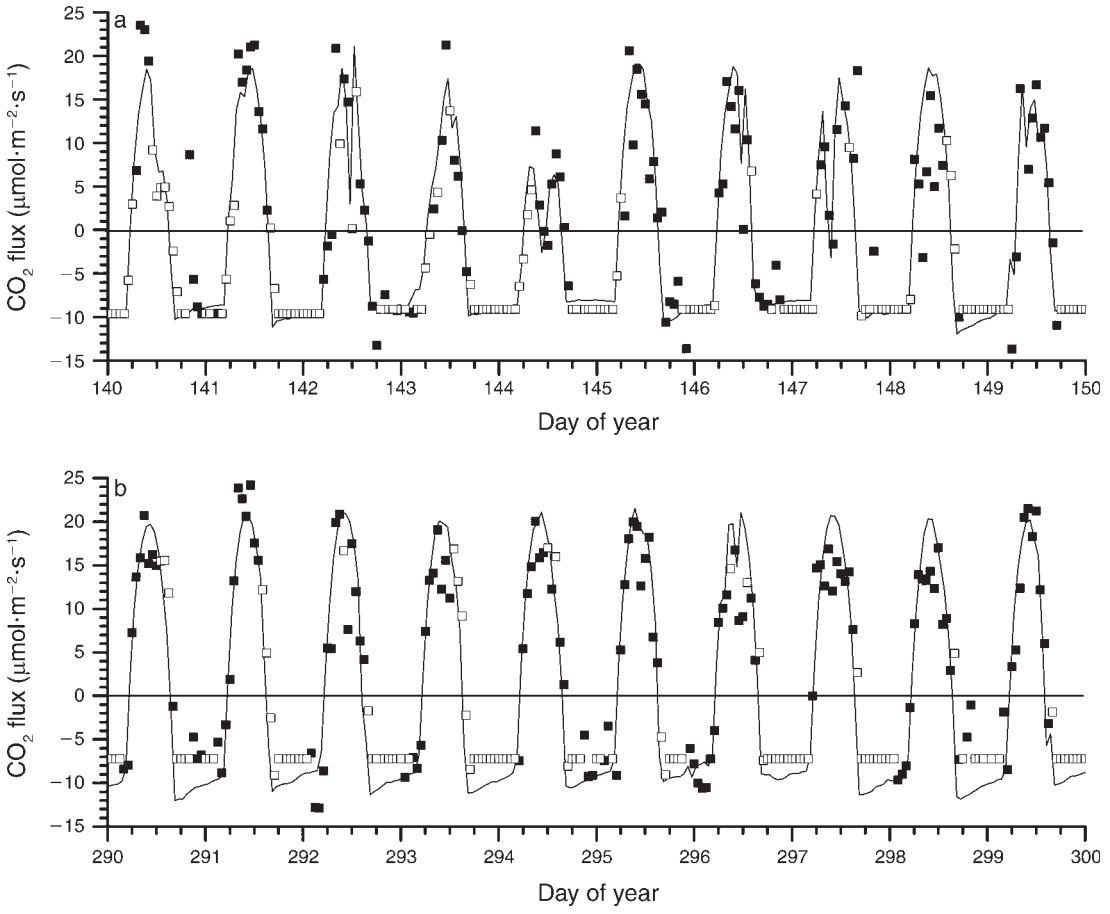

FIG. 5. Carbon dioxide exchange measured (solid symbols), gap-filled (open symbols), and modeled (lines) during (a) the late wet season (day of year [DOY] 141–150) and (b) the late dry season (DOY 290–300) at Santarém km 67 in 2004. Positive values represent downward fluxes, negative values upward ones.

the dry seasons were caused by rises in Q and T_a (Figs. 1a and 2a) that drove rises in CO_2 influxes (Fig. 5). Rises in NEP modeled during the dry seasons were smaller than those in EC-derived NEP because CO_2 effluxes modeled during the dry seasons were larger than gap-filled values (e.g., Fig. 5b).

Annual net ecosystem productivity.—The larger CO_2 effluxes in the model vs. EC measurements (Fig. 5) caused annual GPP and ecosystem respiration, R_{eco}, in the model to exceed those calculated from gap-filled EC fluxes by ~15% during 2002–2004 (Table 3) and those for humid tropical forests worldwide reported by Luyssaert et al. (2007). Similarly, litterfall and R_h were greater than those estimated from biometric measurements in the TNF by Rice et al. (2004) and Pyle et al. (2008). Modeled litterfall and R_h included sources not amenable to biometric measurements, such as root exudation and humus oxidation. Net primary productivity, R_h, and soil respiration (R_{soil}) in the model were also larger than values calculated from biometric and flux chamber measurements for a central Amazonian rain forest reported by Chambers et al. (2004*b*) and for humid tropical forests worldwide reported by Luyssaert et al. (2007). Carbon use efficiency (CUE = NPP/GPP) in the model was 0.38, larger than one of 0.26 for tropical forests reported in Chambers et al. (2004*b*), but smaller than ones of 0.40–0.45 modeled by *ecosys* for temperate and boreal deciduous forests (Grant et al. 2006*a*, *b*). Soil and root respiration in the model were larger than measurements on root exclusion plots in the TNF by Silver et al. (2005).

Net ecosystem productivity in the model was close to that derived from gap-filled EC fluxes by Hutyra et al. (2007) during 2003, 2004, and 2005, as were the CO_2 fluxes from which NEP was derived (Table 2, Fig. 5). Modeled NEP appeared as net gains in aboveground living phytomass (from growth − mortality), offset by losses in standing dead phytomass and in soil organic carbon (SOC). Such an offset was also modeled by Chambers et al. (2004*a*) after accelerated mortality, as could be caused by an ENSO event. Net phytomass gains were slightly larger than those of ~60 ± 40 g C·m^{-2}·yr^{-1} derived from tree measurements by Phillips et al. (1998) and Baker et al. (2004) in other mature Amazonian rain forests. The NEP estimated from biometric measurements in the TNF by Rice et al.

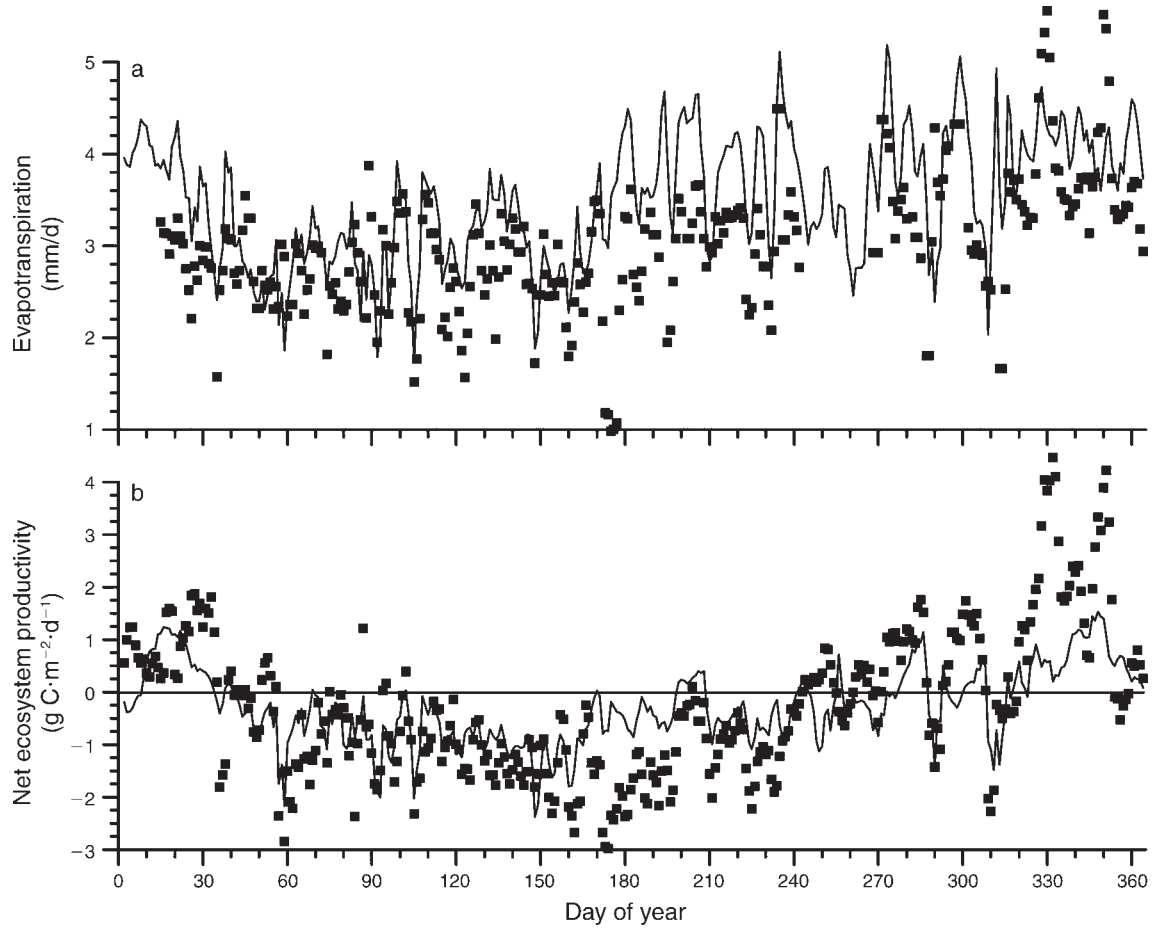

FIG. 6. Three-day moving averages of daily evapotranspiration (ET) and net ecosystem productivity (NEP) modeled (lines) and measured by gap-filled eddy covariance (EC; symbols) at Santarém km 67 during 2003.

(2004) and Pyle et al. (2008) indicated a greater C source, attributed to past disturbances that caused CWD stocks to be larger than expected. However all model and EC values for NEP remained within 100 g $C \cdot m^{-2} \cdot yr^{-1}$ of zero, indicating that this forest stand was likely neither a large sink nor a large source of C.

Centennial net ecosystem productivity.—Aboveground living phytomass in the model rose rapidly following the stand-replacing disturbance with which the model was initialized, attaining stable values of ~20 kg C/m^2 (Fig. 8a) while C_a rose from 275 μmol/mol in 1900 to 375 μmol/mol in 2005. The time course of phytomass growth was determined by mortality and herbivory rates during the model run, as was also shown by Moorcroft et al. (2001). Modeled phytomass was greater than the 14.74 ± 0.59 and 14.8 ± 0.33 kg C/m^2 measured in the TNF during 2001 by Rice et al. (2004) and 2003 by Pyle et al. (2008), indicating that disturbance effects on forest productivity in the TNF may not have been fully represented by the annual mortality of 2% in the model based on Pyle et al. (2008). Stocks of standing dead wood and surface residue (much of it CWD) in the model each stabilized at ~5 kg C/m^2 after 100 years, greater than total CWD stocks measured in the TNF of 4.8 ± 0.5 kg C/m^2 by Rice et al. (2004) during 2001 and 4.0 ± 0.4 kg C/m^2 by Pyle et al. (2008) during 2003. The CWD stocks declined during 2003–2005 (Table 3) as the modeled forest recovered from more rapid mortality during the last ENSO event in 1998. The ratio of annual CWD litterfall (Table 3) to surface CWD stocks indicated a surface litter turnover in the model of 0.12 yr^{-1}, which is in the mid-range of values for CWD of differing densities given in Rice et al. (2004). Fine root mass in the model (from functional equilibrium of σ_C, σ_N, and σ_P exchange between roots and branches described under *Nutrient uptake and translocation* above) varied seasonally from 0.40 to 0.45 kg C/m^2. These root masses were similar to ones of 0.37–0.39 kg C/m^2 measured to a depth of 6 m in the eastern Amazon by Trumbore et al. (2006), although only 0.17 kg C/m^2 of the measured values was considered to be living.

During the first 10 years after stand-replacing disturbance, modeled NEP remained negative (net C source) while litterfall from regenerating phytomass failed to replenish post-disturbance litter stocks declin-

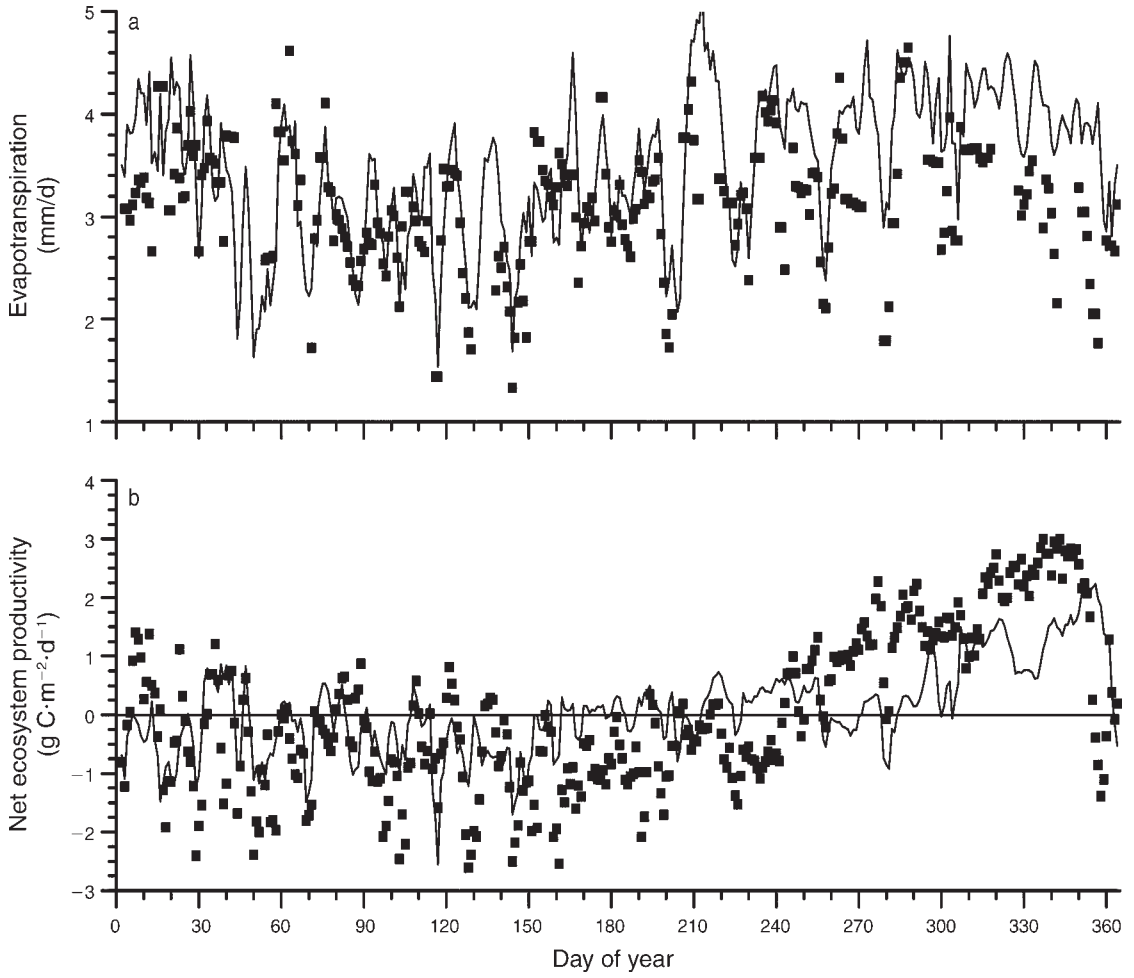

FIG. 7. Three-day moving averages of daily evapotranspiration (ET) and net ecosystem productivity (NEP) modeled (lines) and measured by gap-filled eddy covariance (EC; symbols) at Santarém km 67 during 2004.

ing with R_h (Fig. 8b). This R_h drove initial immobilization and later remineralization of litter P that respectively slowed and later hastened root P uptake, which lowered and then raised foliar P content, CO_2 fixation, and tree growth. Modeled NEP reached maximum values of ~450 g $C \cdot m^{-2} \cdot yr^{-1}$, similar to one of 590 $C \cdot m^{-2} \cdot yr^{-1}$ measured in the central Amazon by Malhi et al. (1998), during rapid tree growth between 10 and 30 years after disturbance. Net ecosystem productivity declined thereafter because rising litterfall from living and dying trees increased litter stocks and hence R_h. This post-disturbance sequence of rising and falling NEP corresponds to that modeled in N-limited temperate (Grant et al. 2007*b*) and boreal (Grant et al. 2006*a*, 2007*a*) forests, but on a contracted timescale because higher temperatures at the TNF hastened organic C, N, and P transformations.

Litterfall modeled in the TNF was accelerated by more rapid mortality (6%) imposed during ENSO years in the model, which hastened transfers from living phytomass to standing dead phytomass and surface residue (Fig. 8a). These transfers raised R_h and thereby lowered NEP for one to two years after each ENSO event (Fig. 8b), after which NEP rose as CWD stocks declined. Successive ENSO events therefore resulted in NEP cycles, the amplitude and duration of which depended on the intensity and frequency of mortality imposed on the model during these events.

DISCUSSION

Modeled vs. measured CO_2 fluxes

The model explained >80% of the variation in >8000 CO_2 fluxes measured by EC over the rain forest at Santarém km 67 during 2003 and 2004 (Table 2). The variation in EC fluxes not explained by the model (15–18%) could be partly attributed to random errors in CO_2 flux measurements estimated by Wesely and Hart (1985) to be ~20%. However, a systematic divergence occurred when modeled CO_2 effluxes exceeded measured and gap-filled values (Fig. 5b), as has been found in other model tests against EC measurements (Grant et al. 2006*a*, *b*).

TABLE 3. Annual carbon budgets (g C/m^2) at km 67 of the Tapajós National Forest (TNF) in Pará, Brazil, modeled by *ecosys* during 2003–2005 and estimated from eddy covariance (EC) and biometric measurements (B).

	2003		2004		2005		Measured
Budget item	*ecosys*	EC	*ecosys*	EC	*ecosys*	EC	B
GPP	3634	3171†	3769	3195†	3751	3206†	3551 ± 160‡ 3000§
R_a							
Shoot	1776		1847		1824		1550§
Root	461		470		465		264–380¶ 550§
Total	2237		2317		2289		2323 ± 144‡ 2100§
NPP							
Shoot	979		1093		1061		693 ± 82¶ 528 ± 61‡ 640§
Root	417		339		401		115 ± 18¶ 77 ± 14¶ 260§ 324 ± 56‡
Total	1397		1452		1462		864 ± 96‡ 900§
Litter							
Shoot, fine	567		578		563		240 ± 50|| 400§
Shoot, coarse	507		504		496		290 ± 26†† 330–475‡‡
Root, fine	43		60		56		37–79¶ 96 ± 7¶
Root, exudates	354		317		341		78§§
Total	1471		1459		1456		
Change in aboveground C							
Living	+18		+121		+101		+140 ± 62|| +77 ± 28†† −80 ± 150¶¶
Dead	−113		−109		−98		
Change in root C	+20		−17		+4		
R_h	1495		1421		1485		570 ± 100|| 492 ± 43†† 877 ± 96† 850§ 705 ± 96¶
R_{soil}	1956		1891		1950		1084 ± 50¶ 1210§
R_{eco}	3732	3262†	3738	3173†	3774	3245†	3061 ± 162‡ 2950§
Change in soil organic C	−27		+31		−38		0 ± 50##
DIC, DOC|||	4		5		8		19 ± 7
NEP	−98	−91 ± 49†	+31	+22 ± 45†	−23	−35 ± 45†	−190 ± 100|| −132 ± 49†† 403 ± 102‡

Note: Abbreviations are: GPP, gross primary productivity; R_a, autotrophic respiration; NPP, net primary productivity; R_h, heterotrophic respiration; R_{soil}, soil respiration; R_{eco}, ecosystem respiration; NEP, net ecosystem productivity.

† From gap-filled EC measurements as described in Hutyra et al. (2008).

‡ Mean values estimated from EC and biometric measurements at 29 humid tropical forest sites by Luyssaert et al. (2007).

§ For central Amazonian forests from Chambers et al. (2004*b*).

¶ Measured in the TNF during 2000 and 2001 by Silver et al. (2005). Net primary productivity and litter were measured to a depth of 0.1 m.

Modeled values for shoot coarse litterfall are from standing dead wood.

|| Aboveground C (= annual growth + recruitment − mortality) and R_h (= respiration by surface coarse woody debris [CWD]) were calculated in the TNF between 1999 and 2001 from Rice et al. (2004).

†† As footnote ||, except from Pyle et al. (2008).

‡‡ Measured in the TNF by Nepstad et al. (2002).

§§ Calculated to a depth of 6 m in eastern Amazonia by Trumbore et al. (2006).

¶¶ From changes in aboveground living phytomass in the TNF between 1984 and 2000 in Miller et al. (2004).

For eastern Amazonian forests from Trumbore et al. (1995).

||| Dissolved inorganic and organic C exported in runoff and drainage water. Measured value from catchment in central Amazon by Waterloo et al. (2006).

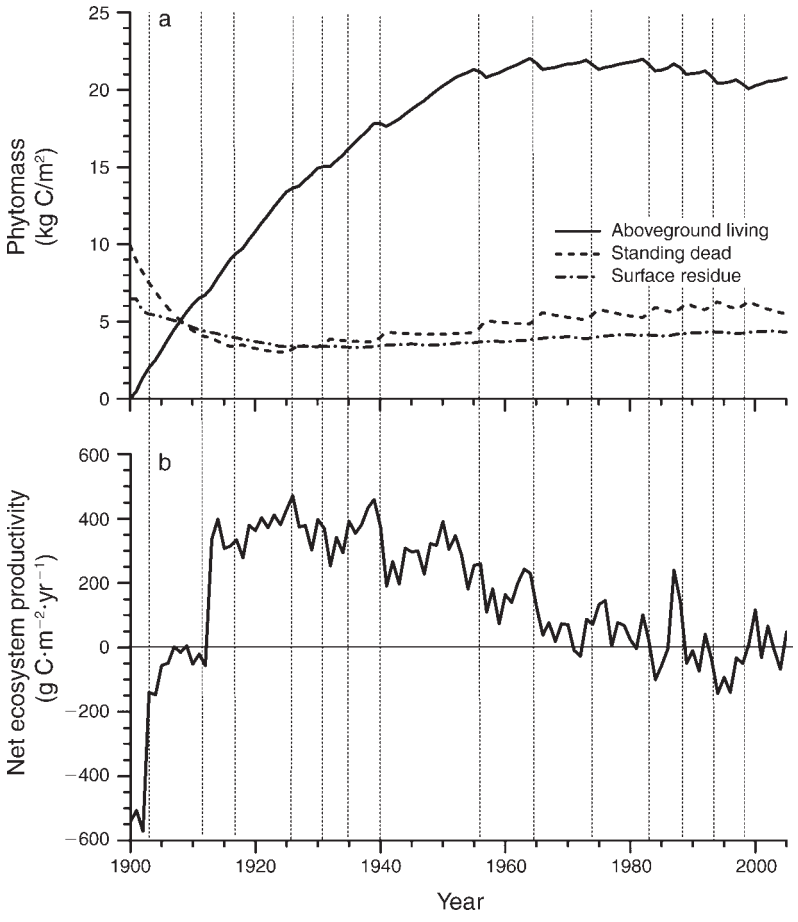

FIG. 8. (a) Aboveground phytomass, standing dead phytomass, and surface residue, and (b) net ecosystem productivity (NEP) modeled during 105 years after a hypothesized stand-replacing disturbance in 1900. Vertical lines indicate El Niño Southern Oscillation (ENSO) event years during which mortality rates in the model were increased.

Some of this excess may be attributed to lower EC effluxes caused by CO_2 loss under stable boundary layers (friction velocity $u^* < 0.22$ m/s) that formed frequently during nights with low wind speeds in the TNF (Miller et al. 2004, Hutyra et al. 2008). Modeled CO_2 effluxes did not systematically diverge from EC values recorded under more turbulent conditions (u^* 0.3–0.8 m/s; e.g., measured EC effluxes in Fig. 5).

In the model, CO_2 effluxes were driven by R_a of CO_2 fixation products σ_C at hourly to daily timescales (Appendix C: Eqs. C.15, C.16) and by R_h of plant litterfall derived from growth products of σ_C at seasonal to interannual timescales (Appendix A: Eq. A.12). Model coefficients used to calculate R_a and R_h were well constrained from basic research in plant and microbial biochemistry (e.g., Waring and Running 1998). Therefore CO_2 effluxes in the model were not independent of CO_2 influxes, but rather were dependent upon these influxes over a range of timescales. Consequently, rises in modeled influxes were followed by rises in modeled effluxes, as during dry vs. wet seasons when modeled and EC influxes rose with radiation and temperature (e.g., Fig. 5b vs. 5a). However, gap-filled effluxes, which are calculated independently of EC influxes, declined during the dry seasons so that gap-filled daily NEP rose above modeled values (Figs. 6b and 7b). Future gap-filling protocol for CO_2 effluxes should perhaps consider preceding CO_2 influxes.

Seasonal effects on energy and CO_2 exchange

There have been several reports that evapotranspiration in Amazonian forests is sustained through the dry season from recovery of water more than 2 m below the soil surface by deep-rooted trees (e.g., Nepstad et al. 1994, da Rocha et al. 2004). Evapotranspiration exceeded precipitation by 190–245 mm during each of the 2002–2005 dry seasons. Given the limited water-holding capacity estimated for this clay-rich soil (0.06–0.10 m^3/m^3 estimated from soil properties in Table 1), uptake to 4–8 m would be necessary during dry seasons to meet precipitation deficits while avoiding plant water stress by depleting less than half of plant available water.

In the model, root length densities used to calculate water uptake in each soil layer were not prescribed, but arose from root growth using the nonstructural products of CO_2 fixation and nutrient uptake. These densities

declined with distance from sources of σ_C in leaves and O_2 in the atmosphere and rose with access to water and nutrients in the soil (Grant 1998). Large belowground transfers of σ_C allowed the root model to maintain sufficient root density for water uptake to depths of 8 m or more during the dry seasons (Fig. 3). This deep rooting enabled peak LE effluxes and CO_2 influxes of greater than 400 W/m^2 and 20 $\mu mol \cdot m^{-2} \cdot s^{-1}$ to be sustained during the entire dry season in the model as was found in EC measurements (Figs. 4 and 5). Seasonality of precipitation therefore had little direct effect on energy and CO_2 exchange, but rather an indirect effect through radiation and temperature (Figs. 6 and 7). However, direct effects of precipitation would be more apparent in the model at sites where deep rooting could not occur, due to inadequate O_2 or water in the soil profile (e.g., compacted, rocky, dry, shallow, or poorly or excessively drained soil) or due to inadequate fixed C to drive root growth caused by disturbances of surface vegetation (e.g., mortality, herbivory, tillage) as in Grant and Flanagan (2007). Spatial aggregation of seasonal effects on CO_2 and energy exchange therefore requires that spatial distributions of key soil profile attributes (e.g., Table 1) and surface disturbances be known or estimated.

Disturbance effects on forest productivity

The *ecosys* model provided a more comprehensive, detailed, and internally consistent estimate of C transformations in this rain forest ecosystem than was possible through EC or biometric measurements alone (Table 3). Both modeled and gap-filled EC fluxes indicated that old-growth stands in the TNF may change between source and sink in different years, but would remain within 100 g $C \cdot m^{-2} \cdot yr^{-1}$ of C neutrality in the absence of major disturbance (Table 3, Fig. 8b). Both modeled and biometrically measured changes in ecosystem C stocks (Table 3) indicated that disturbance could cause old-growth stands to become C sources for some time after disturbance. Saleska et al. (2003) attributed the negative NEP found at Santarém km 67 to a recent episode of rapid mortality, possibly caused by drought associated with an earlier ENSO event. Disturbances such as ENSO events also caused marked reductions in NEP of old-growth forests in the model (Fig. 8a, b). Neither modeled, EC, nor biometric estimates suggest that old-growth stands in the TNF were substantial C sinks.

Long-term model results indicated that forest stands may be substantial C sinks, as found by Malhi et al. (1998), during phytomass regeneration for up to 60 years after stand-replacing disturbances (Fig. 8a, b). The time course of regeneration and rising NEP in the model was affected by the size of CWD stocks left after disturbance (Grant et al. 2007*b*; 10 kg C/m^2 standing, 5 kg C/m^2 surface in this study) which determined the subsequent time course of nutrient immobilization and remineralization during forest regeneration. Modeled NEP eventually declined with nutrient immobilization, approaching C neutrality approximately 70 years after stand replacement. If *ecosys* were used in a regional study of C exchange, a mosaic of stands would be modeled at different stages of the regeneration cycle represented in Fig. 8, depending upon regional disturbance history. A few recently disturbed sites would rapidly emit C, some regenerating sites would rapidly absorb C, and most older sites would slowly emit or absorb C. Depending on the relative contributions of these different sites, the NEP of such a mosaic might be consistent with regional NEP inferred from atmospheric inversion studies that indicated a maximum sink of 150 g $C \cdot m^{-2} \cdot yr^{-1}$ for the central Amazon (Friend et al. 2007).

The time courses of phytomass growth and of NEP were strongly affected by annual mortality and herbivory rates derived from site studies and imposed on the model. Further progress in modeling NEP of Amazonian rain forests will require more detailed estimates of mortality and other disturbances during forest growth cycles under changing weather, as well as a biological basis for modeling mortality and disturbance, perhaps based on depletion of nonstructural C and nutrient reserves caused by high temperatures, water deficits, or herbivory.

Nutrient effects on forest productivity

The productivity of Amazonian rain forests growing on oxisols has been suggested to be limited by available P (Vitousek and Sanford 1986), as apparent from large C:P ratios found in foliage, roots, and litter in the TNF (Silver et al. 2000). Models used to examine ecological controls on Amazonian forest productivity therefore need to be capable of simulating P limitation and the chemical and biological transformations by which it is caused. Further measurements of soil and plant P stocks and transformations need to accompany those of C during forest life cycles in order to constrain modeling of P constraints on forest productivity.

Acknowledgments

Computational facilities for *ecosys* were provided by the University of Alberta and by the Westgrid high-performance computing infrastructure.

Literature Cited

Andreae, M. O., et al. 2002. Biogeochemical cycling of carbon, water, energy, trace gases, and aerosols in Amazonia: the LBA-EUSTACH experiments. Journal of Geophysical Research—Atmospheres 107(D20):8066.

Araújo, A. C., A. D. Nobre, B. Kruijt, J. Elbers, R. Dallarosa, P. Stefani, C. Randow, A. O. Manzi, A. D. Culf, and J. H. C. Gash. 2002. Comparative measurements of carbon dioxide fluxes from two nearby towers in a central Amazonian rainforest: the Manaus LBA site. Journal of Geophysical Research Atmospheres 107(D20):8090.

Baker, T. R., et al. 2004. Increasing biomass in Amazonian forest plots. Philosophical Transactions of the Royal Society B 359:353–365.

Botta, A., N. Ramankutty, and J. A. Foley. 2002. Long-term variations of climate and carbon fluxes over the Amazon basin. Geophysical Research Letters 29:1319.

Bruno, R. D., H. R. da Rocha, H. C. de Freitas, M. L. Goulden, and S. D. Miller. 2006. Soil moisture dynamics in an eastern Amazonian tropical forest. Hydrological Process 20:2477–2489.

Carswell, F. E., et al. 2002. Seasonality in CO_2 and H_2O flux at an eastern Amazonian rain forest. Journal of Geophysical Research—Atmospheres 107(D20):8076.

Chambers, J. Q., N. Higuchi, L. M. Teixeira, J. dos Santos, S. G. Laurance, and S. E. Trumbore. 2004*a*. Response of tree biomass and wood litter to disturbance in a Central Amazon forest. Oecologia 141:596–611.

Chambers, J. Q., E. S. Tribuzy, L. C. Toledo, B. F. Crispim, N. Higuchi, J. Dos Santos, A. C. Araújo, B. Kruijt, A. D. Nobre, and S. E. Trumbore. 2004*b*. Respiration from a tropical forest ecosystem: partitioning of sources and low carbon use efficiency. Ecological Applications 14(Supplement):S72–S88.

Clark, D. A. 2004. Sources or sinks? The responses of tropical forests to current and future climate and atmospheric composition. Philosophical Transactions of the Royal Society 359:477–491.

Coley, P. D., and J. A. Barone. 1996. Herbivory and plant defenses in tropical forests. Annual Review of Ecology and Systematics 27:305–335.

da Rocha, H. R., M. L. Goulden, S. D. Miller, M. C. Menton, L. D. V. O. Pinto, H. C. de Freitas, and A. M. E. S. Figueira. 2004. Seasonality of water and heat fluxes over a tropical forest in eastern Amazonia. Ecological Applications 14(Supplement):S22–S32.

Falcão, N. P. de S., and J. R. A. da Silva. 2004. Caracteristicas de adsorção de fósforo em alguns solos da Amazônia Central. Acta Amazonica 34:337–342.

Friend, A. D., A. Arneth, N. Y. Kiang, M. Lomas, J. Ogée, C. Rödenbeck, S. W. Running, J.-D. Santaren, S. Sitch, N. Viovy, F. I. Woodward, and S. Zaehle. 2007. FLUXNET and modelling the global carbon cycle. Global Change Biology 13:610–633.

Gehring, C., M. Denich, M. Kanashiro, and P. L. G. Vlek. 1999. Response of secondary vegetation in eastern Amazônia to relaxed nutrient availability constraints. Biogeochemistry 45:223–241.

Goulden, M. L., S. D. Miller, H. R. da Rocha, M. C. Menton, H. C. Freitas, A. M. Figueira, and A. C. D. de Sousa. 2004. Diel and seasonal patterns of tropical forest CO_2 exchange. Ecological Applications 14(Supplement):S43–S54.

Grace, J., Y. Malhi, J. Lloyd, J. Mcintyre, A. C. Miranda, P. Meir, and H. S. Miranda. 1996. The use of eddy covariance to infer the net carbon dioxide uptake of Brazilian rain forest. Global Change Biology 2:209–217.

Grant, R. F. 1998. Simulation in *ecosys* of root growth response to contrasting soil water and nitrogen. Ecological Modelling 107:237–264.

Grant, R. F. 2001. A review of the Canadian ecosystem model *ecosys*. Pages 173–264 *in* M. Shaffer, editor. Modeling carbon and nitrogen dynamics for soil management. CRC Press, Boca Raton, Florida, USA.

Grant, R. F. 2004. Modelling topographic effects on net ecosystem productivity of boreal black spruce forests. Tree Physiology 24:1–18.

Grant, R. F., M. Amrani, D. J. Heaney, R. Wright, and M. Zhang. 2004. Mathematical modelling of phosphorus losses from land application of hog and cattle manure. Journal of Environmental Quality 33:210–233.

Grant, R. F., A. G. Barr, T. A. Black, H. Iwashita, J. Kidson, H. McCaughey, K. Morgenstern, S. Murayama, Z. Nesic, N. Saigusa, A. Shashkov, and T. Zha. 2007*a*. Net ecosystem productivity of boreal jack pine stands regenerating from clearcutting under current and future climates. Global Change Biology 13:1423–1440.

Grant, R. F., T. A. Black, D. Gaumont-Guay, N. Kljun, A. G. Barr, K. Morgenstern, and Z. Nesic. 2006*a*. Net ecosystem productivity of boreal aspen forests under drought and climate change: mathematical modelling with *ecosys*. Agricultural and Forest Meteorology 140:152–170.

Grant, R. F., T. A. Black, E. R. Humphreys, and K. Morgenstern. 2007*b*. Changes in net ecosystem productivity with forest age following clearcutting of a coastal Douglas fir forest: testing a mathematical model with eddy covariance measurements along a forest chronosequence. Tree Physiology 27:115–131.

Grant, R. F., and L. B. Flanagan. 2007. Modeling stomatal and nonstomatal effects of water deficits on CO_2 fixation in a semiarid grassland. Journal of Geophysical Research 112: G03011.

Grant, R. F., and D. J. Heaney. 1997. Inorganic phosphorus transformation and transport in soils: mathematical modelling in *ecosys*. Soil Science Society of America Journal 61: 752–764.

Grant, R. F., G. W. Wall, B. A. Kimball, K. F. A. Frumau, P. J. Pinter, Jr., D. J. Hunsaker, and R. L. Lamorte. 1999. Crop water relations under different CO_2 and irrigation: testing of ecosys with the free air CO_2 enrichment (FACE) experiment. Agricultural and Forest Meteorology 95:27–51.

Grant, R. F., Y. Zhang, F. Yuan, S. Wang, P. J. Hanson, D. Gaumont-Guay, J. Chen, T. A. Black, A. Barr, D. D. Baldocchi, and A. Arain. 2006*b*. Intercomparison of techniques to model water stress effects on CO_2 and energy exchange in temperate and boreal deciduous forests. Ecological Modelling 196:289–312.

Hanson, P. J., et al. 2004. Oak forest carbon and water simulations: model intercomparisons and evaluations against independent data. Ecological Monographs 74:443–489.

Harrington, R. A., J. H. Fownes, and P. M. Vitousek. 2001. Production and resource use efficiencies in N- and P-limited tropical forests: a comparison of responses to long-term fertilization. Ecosystems 4:646–657.

Hutyra, L. R., J. W. Munger, E. Hammond-Pyle, S. R. Saleska, N. Restrepo-Coupe, B. C. Daube, P. B. de Camargo, and S. C. Wofsy. 2008. Resolving systematic errors in estimates of net ecosystem exchange of CO_2 and ecosystem respiration in a tropical forest biome. Agricultural and Forest Meteorology 148:1266–1279.

Hutyra, L. R., J. W. Munger, S. R. Saleska, E. Gottlieb, B. C. Daube, A. L. Dunn, D. F. Amaral, P. B. de Camargo, and S. C. Wofsy. 2007. Seasonal controls on the exchange of carbon and water in an Amazonian rainforest. Journal of Geophysical Research—Biogeosciences 112:G03008.

Larcher, W. 2001. Physiological plant ecology. Fourth edition. Springer-Verlag, Berlin, Germany.

Lesack, L. F. W., and J. M. Melack. 1991. The deposition, composition, and potential sources of major ionic solutes in rain of the Central Amazon Basin. Water Resources Research 27:2953–2977.

Luyssaert, S., et al. 2007. CO_2 balance of boreal, temperate, and tropical forests derived from a global database. Global Change Biology 13:2509–2537.

Malhi, Y., A. D. Nobre, J. Grace, B. Kruijt, M. Pereira, A. Culf, and S. Scott. 1998. Carbon dioxide transfer over a central Amazonian rain forest. Journal of Geophysical Research—Atmospheres 103:31593–31612.

McGrath, D. A., M. L. Duryea, and W. P. Cropper. 2001. Soil phosphorus availability and fine root proliferation in Amazonian agroforests 6 years following forest conversion. Agriculture, Ecosystems and Environment 83:271–284.

McGroddy, M. E., W. L. Silver, and R. C. de Oliveira. 2004. The effect of phosphorus availability on decomposition dynamics in a seasonal lowland Amazonian forest. Ecosystems 7:172–179.

Medlyn, B. E., E. Dreyer, D. Ellsworth, M. Forstreuter, P. C. Harley, M. U. F. Kirschbaum, X. Le Roux, P. Montpied, J. Strassemeyer, A. Walcroft, K. Wang, and D. Loustau. 2002. Temperature response of parameters of a biochemically

based model of photosynthesis. II. A review of experimental data. Plant, Cell and Environment 25:1167–1179.

Miller, S. D., M. L. Goulden, M. C. Menton, H. R. Da Rocha, H. C. De Freitas, A. M. E S. Figueira, and C. A. D. De Sousa. 2004. Biometric and micrometeorological measurements of tropical forest carbon balance. Ecological Applications 14(Supplement):S114–S126.

Moorcroft, P. R., G. C. Hurtt, and S. W. Pacala. 2001. A method for scaling vegetation dynamics: the ecosystem demography model (ED). Ecological Monographs 71:557–585.

Nepstad, D. C., et al. 1994. The role of deep roots in the hydrological and carbon cycles of Amazonian forests and pastures. Nature 372:666–669.

Nepstad, D. C., et al. 2002. The effects of partial throughfall exclusion on canopy processes, aboveground production, and biogeochemistry of an Amazon forest. Journal of Geophysical Research 107:8085.

Phillips, O. L., Y. Malhi, N. Higuchi, W. F. Laurance, P. V. Nunez, R. M. Vasquez, S. G. Laurance, L. V. Ferreira, M. S. Stern, S. Brown, and J. Grace. 1998. Changes in the carbon balance of tropical forests: evidence from long-term plots. Science 282:439–442.

Pyle, E. H., et al. 2008. Dynamics of carbon, biomass, and structure in two Amazonian forests. Journal of Geophysical Research—Biogeoscience 113:G00B08.

Rice, A. H., E. H. Pyle, S. R. Saleska, L. Hutyra, M. Palace, M. Keller, P. B. de Camargo, K. Portilho, D. F. Marques, and S. C. Wofsy. 2004. Carbon balance and vegetation dynamics in an old-growth Amazonian forest. Ecological Applications 14(Supplement):S55–S71.

Richardson, A. D., et al. 2006. A multi-site analysis of random error in tower-based measurements of carbon and energy fluxes. Agricultural and Forest Meteorology 136:1–18.

Saleska, S. R., et al. 2003. Carbon in Amazon forests: unexpected seasonal fluxes and disturbance-induced losses. Science 302:1554–1557.

Silver, W. L., J. Neff, M. McGroddy, E. Veldkamp, M. Keller, and R. Cosme. 2000. Effects of soil texture on belowground carbon and nutrient storage in a lowland Amazonian forest ecosystem. Ecosystems 3:193–209.

Silver, W. L., A. W. Thompson, M. E. McGroddy, R. K. Varner, J. D. Dias, H. Silva, P. M. Crill, and M. Keller. 2005. Fine root dynamics and trace gas fluxes in two lowland tropical forest soils. Global Change Biology 11:290–306.

Tian, H. Q., J. M. Melillo, D. W. Kicklighter, A. D. McGuire, J. V. K. Helfrich, B. Moore, and C. J. Vorosmarty. 1998. Effect of interannual climate variability on carbon storage in Amazonian ecosystems. Nature 396:664–667.

Trumbore, S., E. S. Da Costa, D. C. Nepstad, P. B. De Camargo, L. A. Martinelli, D. Ray, T. Restom, and W. Silver. 2006. Dynamics of fine root carbon in Amazonian tropical ecosystems and the contribution of roots to soil respiration. Global Change Biology 12(2):217–229.

Trumbore, S. E., E. A. Davidson, P. B. de Camargo, D. C. Nepstad, and L. A. Martinelli. 1995. Belowground cycling of carbon in forests and pastures of eastern Amazonia. Global Biogeochemical Cycles 9(4):515–528.

Vieira, S., P. B. de Camargo, D. Selhorst, R. da Silva, L. Hutyra, J. Q. Chambers, I. F. Brown, N. Higuchi, J. dos Santos, S. C. Wofsy, S. E. Trumbore, and L. A. Martinelli. 2004. Forest structure and carbon dynamics in Amazonian tropical rain forests. Oecologia 140:468–479.

Vitousek, P. M., and R. L. Sanford. 1986. Nutrient cycling in moist tropical forest. Annual Review of Ecology and Systematics 17:137–167.

von Randow, C., A. O. Manzi, B. Kruijt, P. J. de Oliveira, F. B. Zanchi, R. L. Silva, M. G. Hodnett, J. H. C. Gash, J. A. Elbers, M. J. Waterloo, F. L. Cardoso, and P. Kabat. 2004. Comparative measurements and seasonal variations in energy and carbon exchange over forest and pasture in south west Amazonia. Theoretical and Applied Climatology 78:5–26.

Waring, R. H., and S. W. Running. 1998. Forest ecosystems: analysis at multiple scales. Second edition. Academic Press, San Diego, California, USA.

Waterloo, M. J., S. M. Oliveira, D. P. Drucker, A. D. Nobre, L. A. Cuartas, M. G. Hodnett, I. Langedijk, W. W. P. Jans, J. Tomasella, A. C. de Araujo, T. P. Pimentel, and J. C. M. Estrada. 2006. Export of organic carbon in run-off from an Amazonian rainforest blackwater catchment. Hydrological Processes 20:2581–2597.

Wesely, M. L., and R. L. Hart. 1985. Variability of short term eddy-correlation estimates of mass exchange. Pages 591–612 *in* B. A. Hutchinson and B. B. Hicks, editors. The forest–atmosphere interaction. D. Reidel, Dordrecht, The Netherlands.

APPENDIX A

Key governing equations for simulating net ecosystem productivity in *ecosys*: heterotrophic respiration (*Ecological Archives* M079-016-A1).

APPENDIX B

Key governing equations for simulating net ecosystem productivity in *ecosys*: plant water relations (*Ecological Archives* M079-016-A2).

APPENDIX C

Key governing equations for simulating net ecosystem productivity in *ecosys*: gross primary productivity and autotrophic respiration (*Ecological Archives* M079-016-A3).